J. Fluid Mech. (1990), *vol.* 219, *pp.* 1–23
Printed in Great Britain

Buoyancy-driven instabilities and the nonlinear breakup of a sheared magnetic layer

By FAUSTO CATTANEO[1], TZIHONG CHIUEH[2]† AND DAVID W. HUGHES[3]

[1] Joint Institute for Laboratory Astrophysics, University of Colorado, Boulder, CO 80309, USA

[2] Department of Astrophysical, Planetary and Atmospheric Sciences, University of Colorado, Boulder, CO 80309, USA

[3] Department of Applied Mathematics and Theoretical Physics, University of Cambridge, Silver Street, Cambridge CB3 9EW, UK

(Received 18 May 1989 and in revised form 13 December 1989)

Motivated by problems concerning the storage and subsequent escape of the solar magnetic field we have studied how a magnetic layer embedded in a convectively stable atmosphere evolves due to axisymmetric instabilities driven by magnetic buoyancy. The initial equilibrium consists of a toroidal field sheared by a weaker poloidal component. The linear stability problem is investigated for both ideal and resistive MHD, and the nonlinear evolution is followed by numerical integration of the equations of motion. In all cases we found that the instability is greatly affected by the distribution and strength of the poloidal field. In particular, both the horizontal and vertical scales of the motions are controlled by the location of the surface on which the poloidal field vanishes – the resonant surface. In the nonlinear regime, a resonant surface close to the interface between the magnetized and field-free fluid leads to the localization of the instability so that only a fraction of the magnetic region is disrupted by the motions. By contrast, a deeply seated resonant surface leads to the complete disruption of the layer and to the formation of large, helical magnetic fragments whose identity is preserved for the entire simulation.

1. Introduction

One of the key problems of solar magnetohydrodynamics (MHD) is to explain the mechanism by which the large-scale predominantly toroidal magnetic field escapes from the sun's interior, eventually to appear at the surface as sunspots or smaller magnetic elements. The rapid rise of isolated magnetic flux tubes through the convection zone, together with problems in matching the results of convection-zone dynamo models to the observed solar magnetic field, suggests that the bulk of the toroidal field is not in the convection zone itself but that it may be more readily accommodated in the convectively stable overshoot zone situated beneath the convection zone proper. A full discussion of this matter, along with the appropriate references, may be found in Cattaneo & Hughes (1988, hereinafter referred to as I).

In I we modelled the escape of a magnetic field from the overshoot zone by considering the instabilities of a magnetic layer embedded in a convectively stable atmosphere. To simplify matters we considered the Cartesian analogue of the

† Present address: Institute of Physics and Astronomy, National Central University, Chung-Li, Taiwan.

spherical problem with the y-axis identified with the azimuthal direction, the equilibrium state being piecewise polytropic with a uniform 'toroidal' field $(0, B, 0)$ sandwiched between two non-magnetic regions. The magnetic field, by virtue of its pressure, supports denser fluid above and consequently Rayleigh–Taylor-type instabilities ensue. One of the important results of I was that these primary instabilities lead to secondary Kelvin–Helmholtz instabilities which wrap the gas into regions of strong vorticity and consequently rapidly destroy the coherence of the magnetic field (see, for example, figure 8 of I).

In this paper we undertake a natural extension of the work of I to take account of the fact that the field in the overshoot zone, although predominantly toroidal, will also have a weak poloidal component. The key question that we wish to address by this study is whether the addition of a poloidal ingredient leads to a notable change in the character of the instability. As in I we again work in Cartesian geometry, where a meridional slice of a slightly sheared magnetic field at the equator is transformed into a horizontal field whose direction changes with depth, $(B_x(z), B_y(z), 0)$ say. As explained in I, when the field is purely toroidal, axisymmetric modes $(\partial_y \equiv 0)$ are a good approximation to the most rapidly growing modes, which have a weak dependence on the azimuthal direction (y), and hence in this paper we shall again restrict attention to such modes. It should be noted however that since the field is no longer unidirectional these motions no longer simply interchange magnetic field lines.

The shearing of the field imparts a certain rigidity to the magnetized region, thereby hampering the development of the instability, the precise influence of the shear depending crucially on the manner in which it is distributed. Of particular significance in this field configuration is the possible existence of a so-called *resonant surface* on which the poloidal field vanishes – in axisymmetric geometry the field lines on the surface are purely azimuthal, in our Cartesian model they are purely in the y-direction. As we shall see, the location of the resonant surface plays a crucial role in the evolution of the instability. In linear theory it has a strong influence on both the vertical and horizontal scales of the unstable motions; in the nonlinear regime it determines not only the scale of the escaping field but also the structure of what remains of the magnetic layer after the instability has occurred.

The importance of resonant surfaces in MHD has long been recognized. For instance, resistive MHD instabilities are almost all related to the presence of resonant surfaces near which resistivity plays a crucial role and field line reconnection occurs (see the review by White 1983). In idealized (diffusionless) MHD resonant surfaces again can become of importance if the instability is weak (Rosenbluth, Dagazian & Rutherford 1973). It is important to note though that the instability we have studied is buoyancy-driven and hence of a very different nature to instabilities such as the pinch (e.g. Suydam 1958) which arise from the release of energy stored in curved field lines. In our model there is no potential energy due to magnetic tension, *all* the free energy being gravitational and a consequence of the jump in density at the magnetic interface.

The layout of the paper is as follows. The detailed mathematical formulation of the problem is contained in §2. In §3 we describe two different approaches to the linear stability problem; one using the energy principle of idealized MHD to derive an instability criterion for a particular equilibrium, the other to solve the general linear eigenvalue problem numerically. The results of our fully nonlinear numerical simulations are contained in §4. The concluding §5 discusses our major findings and their possible implications for the solar magnetic field.

2. Mathematical formulation

We consider the development of axisymmetric perturbations of an equilibrium state in which a magnetic layer supports an overlying layer of field-free gas. Both regions in themselves are convectively stable and hence the sole source of potential energy available for instability is the density jump at the magnetic interface. The equilibrium magnetic field is made up of a toroidal component sheared by a weaker poloidal ingredient so that the resulting magnetic field is predominantly azimuthal. As explained in the introduction, the analysis is simplified by adopting a Cartesian model where the coordinate axis y is identified with the azimuthal direction and where the restriction to axisymmetry is translated into the requirement that the solutions be independent of y. The direction of increasing z is taken to be downwards.

The computational domain extends from $z = 0$ (top) to $z = d$ (bottom) and the magnetic field is confined initially below some depth z_t. In the region $z \geqslant z_t$ the equilibrium magnetic field $\boldsymbol{B}_e$ is horizontal and has constant magnitude B_0 but its orientation varies with depth so that it can be written as

$$\boldsymbol{B}_e = \begin{cases} 0, & 0 \leqslant z < z_t, \\ B_0(B_x, (1-B_x^2)^{\frac{1}{2}}, 0), & z_t \leqslant z \leqslant 1. \end{cases} \tag{2.1}$$

In (2.1) the x- and y-components of $\boldsymbol{B}$ are identified with the poloidal and toroidal components respectively. For the moment we wish to keep B_x quite general but allowing the possibility that B_x vanishes for some $z_r \geqslant z_t$, where z_r defines the resonant layer. It is important to realize that in ideal MHD the topology of the resonant surface is preserved by axisymmetric (y-independent) motions and that, therefore, the regions above and below it cannot be brought into contact without reconnection of the field lines. As we shall see, this property has a profound effect on the development of the instability. The existence of a resonant surface in the Cartesian model might seem rather arbitrary since a rotation of the coordinates about the z-axis swaps the 'poloidal' and 'toroidal' components. However, the uniqueness of the resonant surface is ensured by noting that the Cartesian model was constructed as a local representation of an axisymmetric system in spherical geometry where the poloidal and toroidal components are uniquely specified. Throughout the paper, whenever we refer to 'toroidal' ('zonal' or 'azimuthal') or 'poloidal' ('meridional') components of the field or flow, these should be thought of as the local representations in Cartesian geometry of their well-defined counterparts in the spherical system.

The fluid is assumed to be a perfect gas with constant shear viscosity μ, thermal conductivity K, magnetic diffusivity η and principal specific heats c_p and c_v. Initially the atmosphere is piecewise polytropic with a temperature distribution of the form $T = T_0 + \Delta z$. It is convenient to adopt the same units as in I; consequently we choose d as the unit of length and $d/(RT_0)^{\frac{1}{2}}$ as the unit of time, where $R = c_p - c_v$. The evolution equations can then be written as:

$$p = \rho T, \tag{2.2}$$

$$\partial_t \rho + \nabla \cdot \rho \boldsymbol{u} = 0, \tag{2.3}$$

$$\partial_t B + \nabla \cdot (B\boldsymbol{u} - v\boldsymbol{B}) = \tau C_k \nabla^2 B, \tag{2.4}$$

$$\partial_t A + \boldsymbol{u} \cdot \nabla A = \tau C_k \nabla^2 A, \tag{2.5}$$

$$\partial_t \rho \boldsymbol{u} + \nabla \cdot \rho \boldsymbol{u}\boldsymbol{u} = -\nabla p + (m+1)\,\theta \rho \hat{\boldsymbol{z}} + C_k \sigma(\nabla^2 \boldsymbol{u} + \tfrac{1}{3}\nabla(\nabla \cdot \boldsymbol{u})) - (\nabla^2 A \nabla A + \tfrac{1}{2}\nabla B^2 + \nabla A \times \nabla B)/\beta, \tag{2.6}$$

$$\rho(\partial_t T + \boldsymbol{u} \cdot \nabla T) + (\gamma - 1)\, p \nabla \cdot \boldsymbol{u} = \gamma C_k \nabla^2 T + (\gamma - 1)\, C_k(\sigma \phi_{ij} \partial_i u_j + \tau(\nabla \times \boldsymbol{B})^2/\beta), \tag{2.7}$$

where $\phi_{ij} = \partial_i u_j + \partial_j u_i - \frac{2}{3}\delta_{ij} \nabla \cdot \boldsymbol{u}$, $\boldsymbol{B} = (-\partial_z A, B, \partial_x A)$ and $\boldsymbol{u} = (u, v, w)$. As in I the six dimensionless parameters are defined by:

$$\sigma = \frac{\mu c_p}{K}, \quad \tau = \frac{\eta \rho_0 c_p}{K}, \quad \beta = \frac{\mu_0 p_0}{B_0^2},$$

$$m = \left(\frac{g}{R\Delta} - 1\right), \quad \theta = \frac{\Delta d}{T_0}, \quad C_k = \frac{K}{\rho_0 c_p d (RT_0)^{\frac{1}{2}}}.$$

We assume that the fields and motions are periodic in the x-direction and adopt the following conditions on the horizontal boundaries:

$$T = 1, \quad A = 0 \quad \text{at} \quad z = 0 \quad \text{and} \quad T = 1 + \theta, \quad A = A_0 \quad \text{at} \quad z = 1;$$

$$w = \partial_z u = \partial_z v = \partial_z B = 0 \quad \text{at} \quad z = 0, 1;$$

where the constant A_0 depends on the distribution of the poloidal flux, which will be specified later. These boundary conditions correspond to impenetrable, stress-free, perfectly conducting walls (thermally). It is easy to show that the conditions on A and B imply that both the toroidal and poloidal fluxes are conserved.

The numerical techniques used to solve (2.2)–(2.7) in both the linear and nonlinear regimes were a natural extension of those of I.

3. Linear theory

In this section we study the linear stability problem for the twisted field. Two approaches, one based on the energy principle, the other on the solutions of the linearized equations, are used to calculate, respectively, the conditions for marginal stability and the growth rate as a function of the defining parameters. It is important to distinguish between the two methods. The first concentrates on the most unstable mode, i.e. the one requiring the least driving to be destabilized, which for our problem has vanishing horizontal wavenumber. The second calculates the mode of maximum growth rate which, typically, has finite horizontal wavenumber.

3.1. *The ideal MHD case*

In this subsection we derive the condition of marginal stability for sheared magnetic layers in the special case of no diffusion – ideal MHD. This result concerns the absolute stability of the layer and we defer the calculation of the growth rate's dependence on horizontal wavenumber to the next section where the non-ideal case is considered. As we shall see, the presence of a resonant surface plays a crucial role for the marginally stable modes. The resonant surface corresponds to the location where the magnetic tension vanishes and the Alfvén wave becomes infinitely slow. The surface behaves so plastically that it can absorb any plasma displacement, thus insulating the perturbations on either side of the resonant surface. This insulation favours instability, as the unstable motions can be confined to the regions where the free energy is positive.

The derivation makes use of the energy principle of Bernstein *et al.* (1958) which expresses the change in the potential energy of the system due to a small Lagrangian displacement ξ from equilibrium. Letting δW be the change in potential energy we write

$$\delta W = -\frac{1}{2} \int_V \xi \cdot \boldsymbol{F}(\xi) \, \mathrm{d}V, \tag{3.1}$$

where $$\boldsymbol{F}(\boldsymbol{\xi}) = \boldsymbol{\nabla}(\gamma p \boldsymbol{\nabla}\cdot\boldsymbol{\xi} + \boldsymbol{\xi}\cdot\boldsymbol{\nabla}p) + \frac{1}{\beta}(\boldsymbol{J}\times\boldsymbol{Q} - \boldsymbol{B}\times(\boldsymbol{\nabla}\times\boldsymbol{Q})) + (m+1)\,\theta\boldsymbol{\nabla}\cdot(\rho\boldsymbol{\xi})\,\boldsymbol{e}_z, \quad (3.2a)$$

and $$\boldsymbol{Q} = \boldsymbol{\nabla}\times(\boldsymbol{\xi}\times\boldsymbol{B}). \quad (3.2b)$$

Since $\boldsymbol{F}(\boldsymbol{\xi})$ is both self-adjoint (see Kulsrud 1964) and linear in $\boldsymbol{\xi}$ the marginality condition is obtained through the formal minimization of δW which involves the construction of a non-trivial displacement for which $\delta W = 0$.†

Assuming that the equilibrium configuration is in hydrostatic balance and that $\boldsymbol{\xi} = (\xi_x(z)\sin lx, \xi_y(z)\cos lx, \xi_z(z)\cos lx)$ we can write

$$\delta W = \frac{1}{2}\int \mathrm{d}z \left\{ \frac{1}{\beta}\left(B_x^2\left(\frac{\mathrm{d}\xi_z}{\mathrm{d}z}\right)^2 + B_y^2\left(l\xi_x + \frac{\mathrm{d}\xi_z}{\mathrm{d}z}\right)^2 + l^2 B_x^2\,\xi_y^2 - 2lB_x B_y\,\xi_y\left(l\xi_x + \frac{\mathrm{d}\xi_z}{\mathrm{d}z}\right) + l^2 B_x^2\,\xi_z^2\right) \right.$$
$$\left. + \gamma p\left(l\xi_x + \frac{\mathrm{d}\xi_z}{\mathrm{d}z}\right)^2 + (m+1)\,\theta\xi_z\left(2\rho\left(l\xi_x + \frac{\mathrm{d}\xi_z}{\mathrm{d}z}\right) + \frac{\mathrm{d}\rho}{\mathrm{d}z}\xi_z\right)\right\}, \quad (3.3)$$

after performing the integration in x. Minimizing with respect to ξ_x and ξ_y gives

$$\delta W = \frac{1}{2}\int \mathrm{d}z \left\{ \frac{1}{\beta}\left(B_x^2\left(\frac{\mathrm{d}\xi_z}{\mathrm{d}z}\right)^2 + l^2 B_x^2\,\xi_z^2\right) + (m+1)\,\theta\Gamma(z)\,\xi_z^2\right\}, \quad (3.4)$$

where $\Gamma(z) = \mathrm{d}\rho/\mathrm{d}z - (m+1)\,\theta\rho^2/\gamma p$, which for our piecewise polytropic equilibrium takes the form

$$\Gamma(z) = \begin{cases} \theta\left(\dfrac{\gamma m - m - 1}{\gamma}\right)(1+\theta z)^{m-1}, & 0 \leqslant z < z_t, \quad (3.5a) \\ \theta\dfrac{(\gamma m - m - 1)}{\gamma(1+\theta z_t)^{m+1}}(1+\theta z)^{m-1} - \dfrac{\delta(z-z_t)}{2\beta(1+\theta z_t)}, & z_t \leqslant z \leqslant 1. \quad (3.5b) \end{cases}$$

In (3.5) the term $(\gamma m - m - 1)/\gamma$ is the subadiabatic gradient, which gives a local measure of the stability of the fluid to vertical displacements. The last term in (3.5*b*) measures the potential energy available to the system by virtue of the density jump at the magnetic interface. It should be noted that the limit $B_x \to 0$ in (3.4) does not yield the correct expression for interchange modes since in the minimization process we have assumed that $\xi_y \neq 0$. The limit $B_x \to 0$ in fact gives the expression for undular modes with zero wavenumber in the y-direction (see Hughes & Cattaneo 1987).

We proceed with the formal minimization of (3.4) with respect to ξ_z subject to the boundary conditions $\xi_z(0) = \xi_z(1) = 0$. The layer is divided into three regions defined as follows:

Region I	$0 \leqslant z < z_t$	from the upper boundary to the magnetic interface;
Region II	$z_t \leqslant z < z_r$	from the magnetic interface to the resonant layer;
Region III	$z_r \leqslant z \leqslant 1$	from the resonant layer to the lower boundary;

and the behaviour of δW in each region is considered in turn. It will become apparent that the contribution to $\delta W_{\min}$ arising from region III vanishes identically while that from region I, though positive, can be made arbitrarily small and that, therefore, the marginality condition is determined mainly by the behaviour of ξ_z in region II.

† The actual quantity to be minimized is $L = \delta W - \lambda\int|\boldsymbol{\xi}|^2\,\mathrm{d}z$, where the Lagrangian multiplier λ can be interpreted as the square of the growth rate. Since we are concerned with the condition for marginal stability we set $\lambda = 0$.

Integrating (3.4) by parts over region II gives

$$\delta W_{\mathrm{II}} = \frac{1}{2\beta}\left\{\left[B_x^2 \frac{\mathrm{d}\xi_z}{\mathrm{d}z}\xi_z\right]_{z_t}^{z_r} - \frac{(m+1)\,\theta\xi_z^2(z_t)}{2\beta(1+\theta z_t)} - \int_{z_t}^{z_r} \mathrm{d}z\,\xi_z\left(\frac{\mathrm{d}}{\mathrm{d}z}\left(B_x^2\frac{\mathrm{d}\xi_z}{\mathrm{d}z}\right) - (l^2B_x^2+\beta(m+1)\,\theta\Gamma(z))\,\xi_z\right)\right\}. \quad (3.6)$$

The first two terms in (3.6) are the contributions to δW_{II} arising from the magnetic interface while the integrand gives rise to the Euler–Lagrange equation for δW. The minimization requires that both the boundary terms and the integral vanish independently. In order to obtain an explicit solution of the Euler–Lagrange equation we introduce some simplifying assumptions; namely that θ is small and that, therefore, the stratification is weak and the equilibrium thermodynamic quantities are approximately constant. Assuming further that $B_x = B_x'(z-z_r)$, the Euler–Lagrange equation can be written as

$$\frac{\mathrm{d}}{\mathrm{d}\zeta}\left(\zeta^2\frac{\mathrm{d}\xi_z}{\mathrm{d}\zeta}\right) - (\zeta^2+\alpha^2)\,\xi_z = 0, \quad (3.7a)$$

where we have introduced the variable $\zeta = l(z_r - z)$ and the constant

$$\alpha^2 = \frac{\beta(m+1)\,\theta^2(\gamma m - m - 1)}{\gamma B_x'^2}. \quad (3.7b)$$

Equation (3.7a) has the regular solution

$$\xi_z = \zeta^{-\frac{1}{2}} I_{\nu+\frac{1}{2}}(\zeta), \quad (3.8)$$

where I is the modified Bessel function. Since, from consideration of the effects of magnetic tension, we expect the modes with small l to be more readily destabilized, it suffices that in establishing a criterion for absolute stability we examine the behaviour of (3.8) for small ζ. It is therefore helpful to express the solution (3.8) as the power series

$$\xi_z(\zeta) = \zeta^\nu G_\nu(\zeta), \quad (3.9a)$$

where

$$\nu = \tfrac{1}{2}[(4\alpha^2+1)^{\frac{1}{2}} - 1] > 0 \quad (3.9b)$$

and

$$G_\nu(\zeta) = 1 + \sum_{j=1}^{\infty} \frac{\zeta^{2j}}{\prod_{n=1}^{j}(2n(2n+1+2\nu))}. \quad (3.9c)$$

The positive definite function $G_\nu(\zeta)$ is monotonic in ζ and satisfies

$$\frac{\mathrm{d}}{\mathrm{d}\zeta}G_\nu(\zeta) \geqslant 0 \quad (3.10)$$

with the equality holding at $\zeta = 0$, a property that we shall use presently.

Having obtained an explicit expression for the displacement in region II we now justify our previous statement that the contributions from regions I and III can be neglected. We may assume that the displacement vanishes identically in region III since this choice satisfies both the Euler–Lagrange equation and the boundary condition at $z = 1$. Furthermore the trivial solution in region III satisfies the matching condition with the solution in region II since both the displacement and $(B_x^2(\mathrm{d}/\mathrm{d}z)\,\xi_z^2)$ vanish as z_r is approached from above. In region I we cannot assume that ξ_z vanishes identically since $\xi_z|_{z_t}$ is non-zero. The integrand of (3.4) is positive definite in region I and hence by choosing a displacement that decays sufficiently rapidly above the magnetic interface while matching smoothly to ξ_z in region II, δW_{I}

can be made arbitrarily small. Consequently the marginality condition is determined solely by the behaviour of ξ_z in region II.

The condition that δW vanishes can now be written as

$$B_x^2(z_t)\left(\frac{\mathrm{d}}{\mathrm{d}z}\ln\xi_z\right)\Big|_{z_t} = -\tfrac{1}{2}(m+1)\,\theta, \tag{3.11}$$

where we observe that the boundary term coming from $z = z_r$ in equation (3.6) is identically zero since ν is positive. Substituting for ξ_z in (3.11) from (3.9), and noting that G_ν is an even function of ζ, we obtain the marginality condition

$$\frac{\nu}{(z_r - z_t)} + \frac{\mathrm{d}}{\mathrm{d}z}\ln G_\nu(l(z-z_r))|_{z_t} = \frac{(m+1)\,\theta}{2B_x^2(z_t)}. \tag{3.12}$$

The second term in (3.12) is positive definite and, by property (3.10), also monotonically increasing in l, thereby confirming our expectation that the modes with small l are the most readily destabilized. After substituting for ν from (3.9*b*) and (3.7*b*), and rearranging, we derive the condition

$$4\beta\frac{(\gamma m - m - 1)}{\gamma} > \frac{(m+1)}{(\delta B_x)^2} + \frac{2}{\theta D} \quad \text{for stability,} \tag{3.13}$$

where δB_x is the shear at the magnetic interface and D is the distance between the resonant layer and the interface. Expression (3.13) shows that stability is aided by large magnetic shears and large subadiabtic gradients, as is to be expected. Rather more surprising is that (3.13) implies the existence of a critical β given by

$$\beta_c = \frac{\gamma}{2(\gamma m - m - 1)\,\theta D}, \tag{3.14}$$

below which no amount of shear can stabilize the layer. The presence of D in the denominator also indicates that the closer the resonant surface is to the magnetic interface the harder it is to achieve stability.

This section is concluded by extending our results to the case where B_x never vanishes within the magnetic layer and therefore there is no resonant surface. In this case region III is absent and region II extends to the lower boundary where ξ_z must satisfy the condition $\xi_z|_1 = 0$. Without loss of generality we consider a case where the shear increases with depth and write, for simplicity, $B_x = B_x' z$. The Euler–Lagrange equation in region II is unchanged so that (3.11) still gives the marginality condition, only now the expression for ξ_z contains also the singular solution of (3.7*a*). To lowest order in l we can write

$$\xi_z \sim (lz)^\nu - l^{2\nu+1}(lz)^{-(\nu+1)}, \tag{3.15}$$

which clearly satisfies the boundary condition $\xi_z|_1 = 0$. Substituting (3.15) into (3.11) gives

$$\frac{\nu z_t^\nu + (\nu+1)\,z_t^{-(\nu+1)}}{z_t^{-(\nu+1)} - z_t^\nu} > \frac{(m+1)\,\theta z_t}{2B_x^2(z_t)} \quad \text{for stability.} \tag{3.16}$$

Although the stability criterion is more involved, the stabilizing effects of the lower boundary condition are apparent in the denominator of the left-hand side which becomes small as $z_t \to 1$.

3.2. *The general case*

In the previous subsection we made use of the energy principle to determine the influence of the poloidal field (and, in particular, to determine the significance of the resonant layer) for the special case of ideal MHD. This complementary section considers the more general problem arising from the linearized versions of the

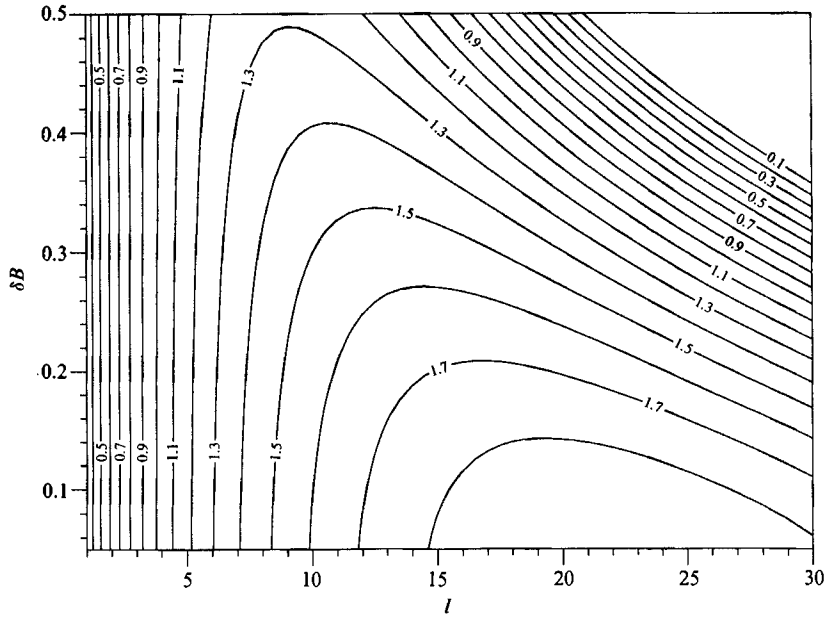

FIGURE 1. Contour plot of the growth rate of the most unstable mode as a function of the poloidal excursion δB and the horizontal wavenumber l. The resonant layer is fixed at $z_r = 0.7$. $\gamma = \frac{5}{3}$, $m = 1.6$, $\tau = 0.01$, $C_k = \sigma = 0.05$, $\theta = 2$, $\beta = 0.5$, $z_t = 0.4$.

governing equations (2.2)–(2.7). In contrast to §3.1 all of the diffusivities are non-zero and no simplifying assumptions are made concerning the initial equilibrium – the price we pay for this enhanced generality is that solutions can only be obtained numerically.

All of the results of this section were derived from an initial field profile given by (2.1) with the following linear variation of B_x:

$$B_x = \delta B \frac{(z - z_r)}{(1 - z_t)}, \tag{3.17}$$

where δB is the total excursion of the poloidal field $(B_x(1) - B_x(z_t))$ and z_r is the position of the resonant layer. (We have also considered parabolic profiles of the form (4.1*b*) where both B_x and its first derivative vanish at $z = z_r$; although the significance of the resonant surface is enhanced for such fields, we found the structure and growth rates of the linear eigenmodes to differ only slightly from those arising from the linear profile (3.17).) As in I, guided by the astrophysical nature of the problem, we shall consider only small values of σ, τ and C_k (of course for a well-posed problem τ *must* be small so as to prevent the rapid diffusion of the initial field profile) – as expected on physical grounds the bifurcation to instability is then always steady. In order that the vertical structure of the eigenfunctions be illustrated clearly we shall, for this section, set $z_t = 0.4$; for the nonlinear simulations of §4 higher values of z_t were adopted so as to leave ample room for the instability to evolve.

In keeping with the underlying theme of the paper we shall concentrate mainly on the novel features arising from the introduction of a poloidal field. The eigenfunctions are strongly peaked near z_t (as in the absence of B_x), reflecting the jump in density there, but their vertical structure, horizontal scale and growth rates are also strongly influenced by variations in δB and z_r. The contour plot of figure 1 shows the variation in the growth rate as a function of δB and the horizontal wavenumber l for a given

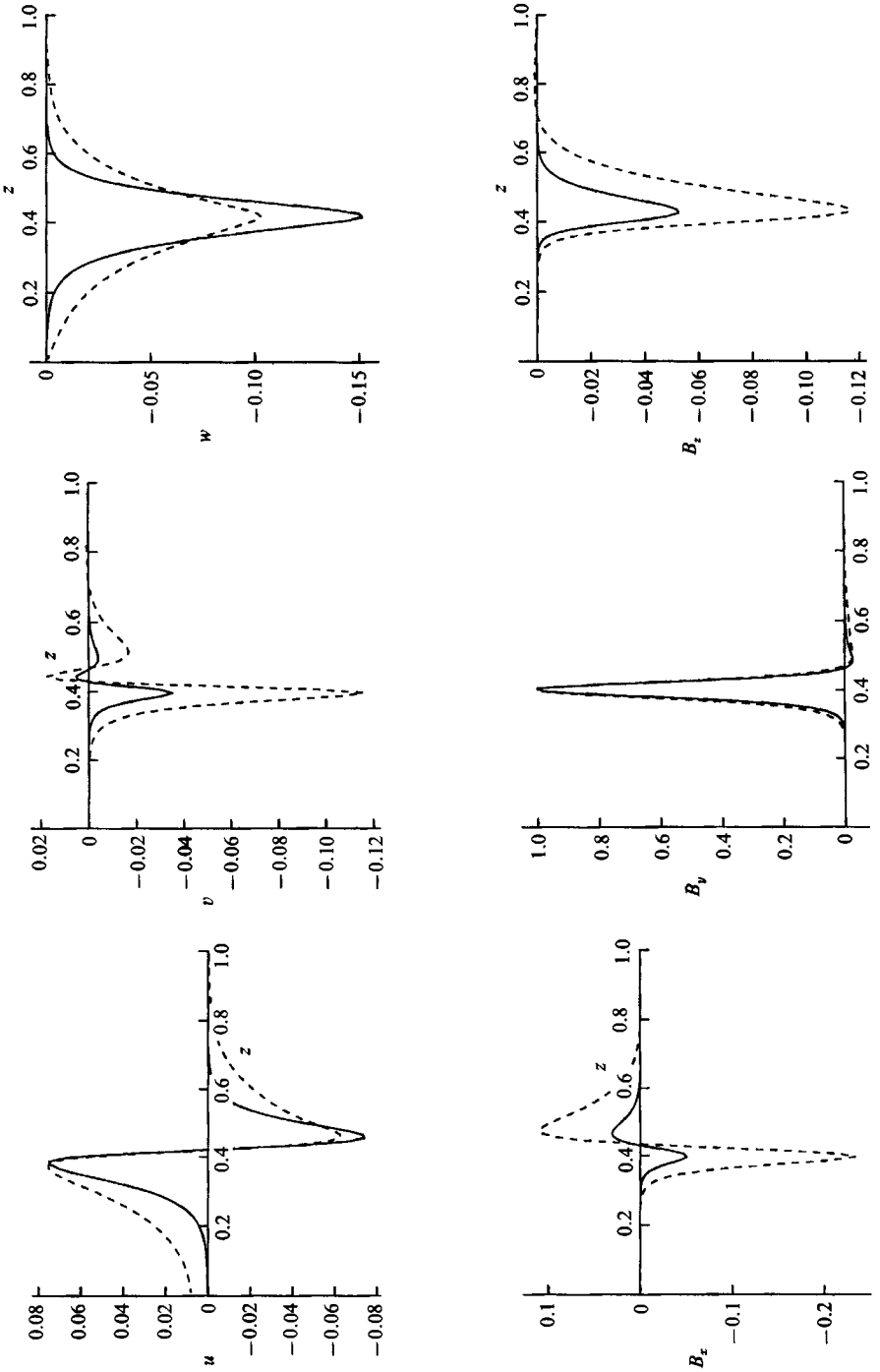

FIGURE 2. Comparison of the eigenfunctions of the most rapidly growing modes for a fixed resonant layer ($z_r = 0.7$) and two different values of the poloidal excursion δB. The solid lines correspond to $\delta B = 0.1$, $l = 20.8$; the dashed lines to $\delta B = 0.5$, $l = 8.9$. $\gamma = \frac{5}{3}$, $m = 1.6$, $\tau = 0.01$, $C_k = \sigma = 0.05$, $\theta = 2$, $\beta = 0.5$, $z_t = 0.4$.

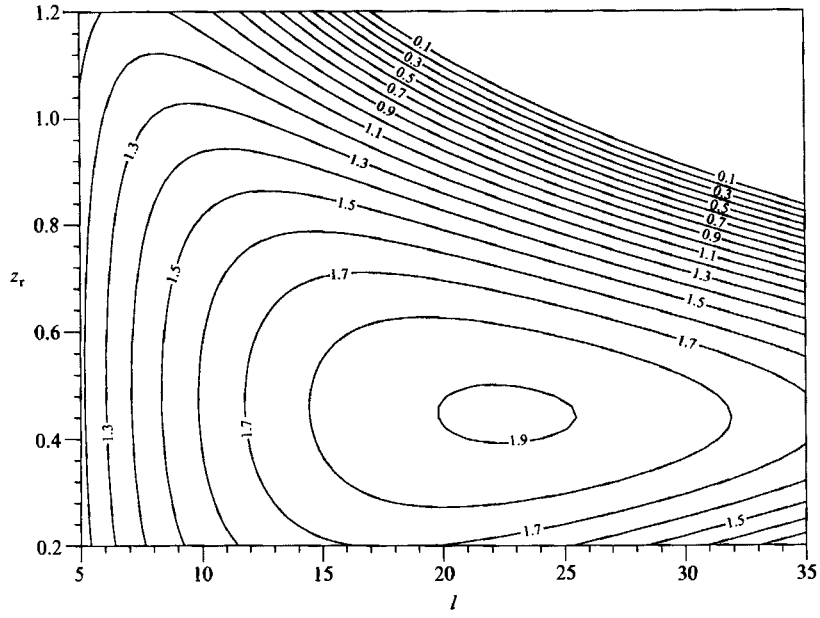

FIGURE 3. Contour plot of the growth rate of the most unstable mode as a function of the depth of the resonant layer z_r and the horizontal wavenumber l. The poloidal excursion $\delta B = 0.2$. $\gamma = \frac{5}{3}$, $m = 1.6$, $\tau = 0.01$, $C_k = \sigma = 0.05$, $\theta = 2$, $\beta = 0.5$, $z_t = 0.4$.

depth of the resonant layer, $z_r = 0.7$. When the poloidal field is weak (δB small) the most unstable modes are approximately interchanges with only a small 'azimuthal' flow v and small perturbations to the 'meridional' field (see the solid eigenfunctions of figure 2). The vertical structure is determined principally by the location of the magnetic interface, the horizontal scale by diffusive effects (see I); obviously when the poloidal field is weak its precise distribution (determined by z_r) is not a significant factor. Increasing the strength of B_x is stabilizing and also brings about changes in the structure of the eigenfunctions. The modes most effective at counteracting the stabilizing poloidal field are of greater vertical extent than the quasi-interchanges favoured for weak fields, reaching down to the resonant layer where the poloidal field vanishes. This may be seen by inspection of the dashed eigenfunctions in figure 2 which also show how v and the perturbations to B_x and B_z are significantly increased.† The effects of the magnetic tension, virtually negligible for the interchange-like modes favoured when B_x is small, are of course brought into prominence as B_x is increased – as a result the fastest-growing modes assume a larger horizontal scale as may be seen from figure 1.

The contour plot of figure 3 depicts the variation in growth rate as a function of l and z_r for a fixed value of δB. It should be noted that there are values of z_r less than z_t or greater than 1 – for such cases equation (3.17) is still a perfectly sensible definition of the field profile, it just means that there is no resonant surface as such. When $z_r < z_t$, $|B_x|$ just increases with depth in the region $z_t < z < 1$; when $z_r > 1$, $|B_x|$ decreases with depth in $z_t < z < 1$ (though never becoming zero). It can be seen that in agreement with the ideal MHD results of §3.1, instability is most easily achieved when the resonant surface is close to the top of the magnetic layer ($z_r \approx z_t$). For such cases, no matter how strong the poloidal field may become at greater depth, the

† As in I we actually adopted a slightly smeared version of (3.17) as the initial field profile, thus accounting for the eigenfunctions of $\boldsymbol{B}$ being non-zero for $z < z_t$.

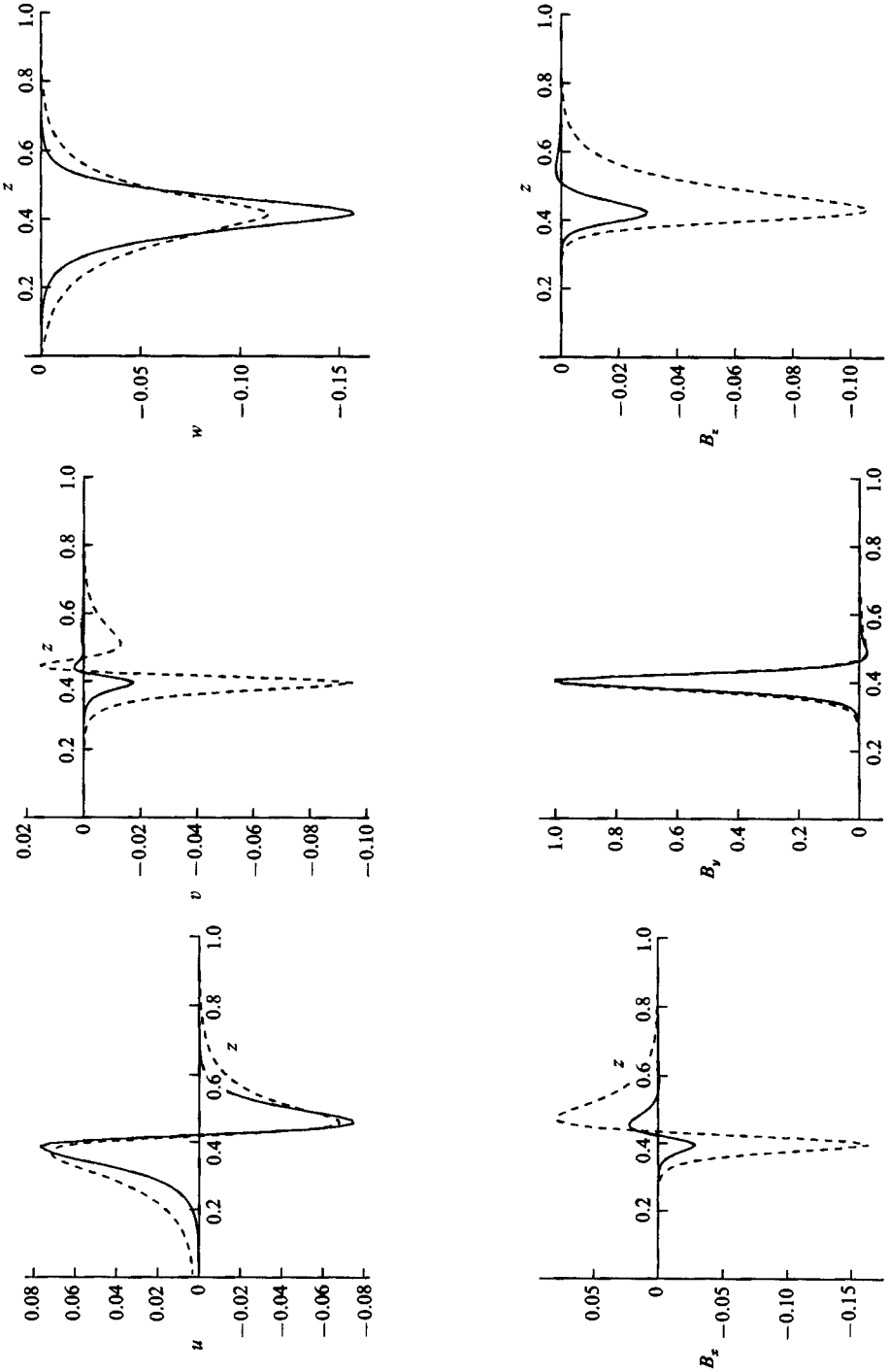

FIGURE 4. Comparison of the eigenfunctions of the most rapidly growing modes for a fixed excursion ($\delta B = 0.2$) and two different positions of the resonant surface. The solid lines correspond to $z_r = 0.5$, $l = 22.1$; the dashed lines to $z_r = 0.9$, $l = 12.0$. $\gamma = \frac{5}{3}$, $m = 1.6$, $\tau = 0.01$, $C_k = \sigma = 0.05$, $\theta = 2$, $\beta = 0.5$, $z_i = 0.4$.

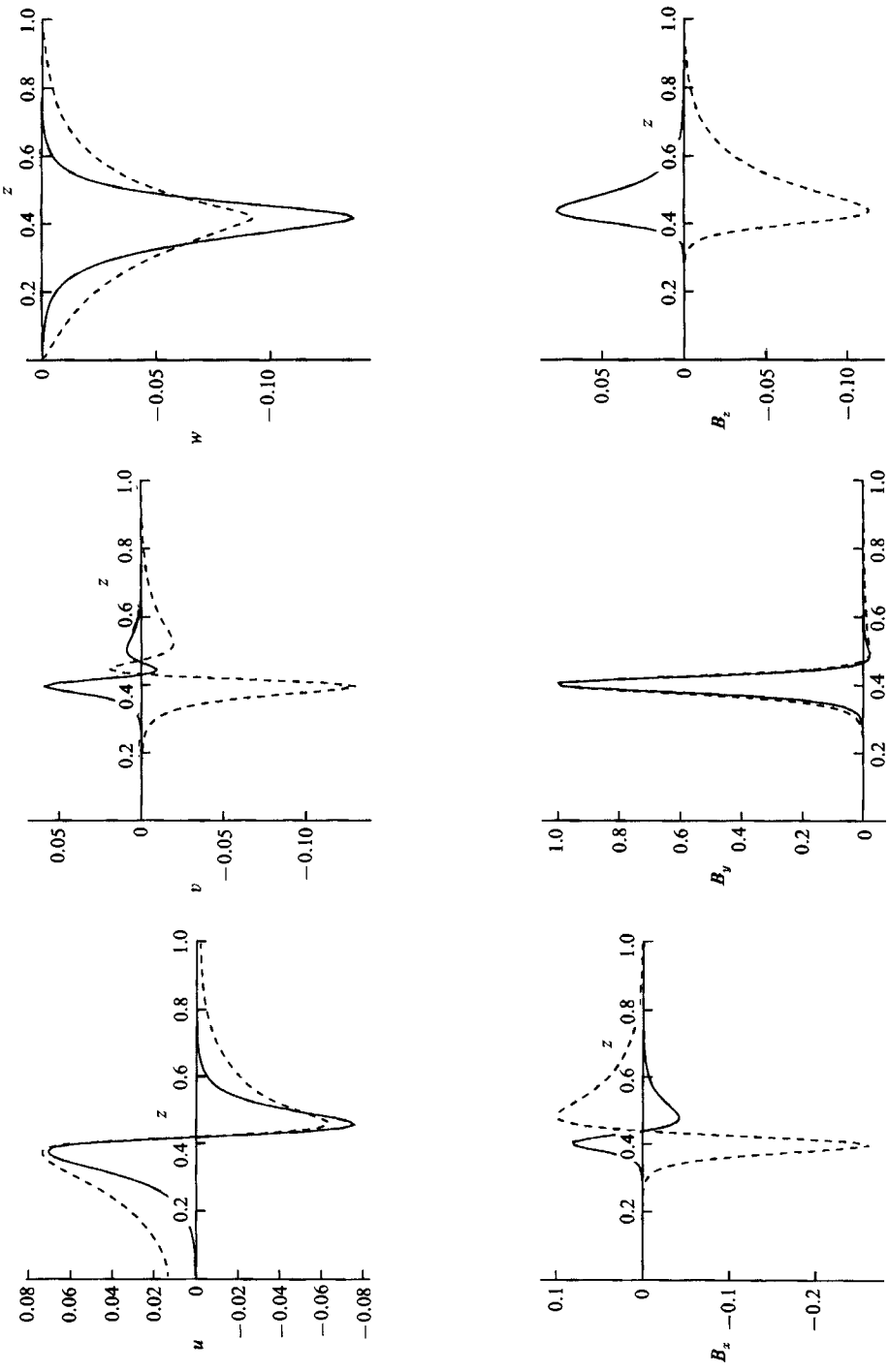

FIGURE 5. Comparison of the eigenfunctions of the most rapidly growing modes for a fixed excursion ($\delta B = 0.2$) and two different positions of the resonant surface. The solid lines correspond to $z_r = 0.2$, $l = 17.9$; the dashed lines to $z_r = 1.2$, $l = 7.3$. $\gamma = \frac{5}{3}$, $m = 1.6$, $\tau = 0.01$, $C_k = \sigma = 0.05$, $\theta = 2$, $\beta = 0.5$, $z_i = 0.4$.

instability always exploits the weak poloidal field near the top of the magnetic region by assuming the form of small-scale (both vertical and horizontal) quasi-interchange modes. If the resonant layer is positioned deeper within the magnetic region ($z_t < z_r < 1$) then the preferred eigenfunctions have a greater vertical extent, thereby again exploiting the weak poloidal field near z_r. Figure 4 shows a comparison between the eigenfunctions for the two cases of the resonant layer close to the magnetic interface (solid line) and close to the bottom boundary (dashed line). In the light of the physical arguments above it is not too surprising that figure 2, which is a comparison of eigenfunctions for different δB at a fixed z_r, and figure 4, a comparison of different z_r for fixed δB, are somewhat similar.

When $z_r < z_t$ the poloidal field never vanishes and its magnitude increases linearly with depth. The preferred modes are confined close to z_t where the poloidal field is weakest; as can be seen from figure 3, as z_r is reduced below z_t, thus increasing the poloidal field strength throughout the magnetic layer, the increased magnetic tension brings about an increase in the horizontal scale of the favoured modes. When $z_r > 1$ the poloidal field again never vanishes and its magnitude decreases linearly with depth. As is to be expected, compared with the case of $z_r < z_t$, this allows for greater penetration into the magnetic layer. This feature is illustrated by figure 5 which contrasts the eigenfunctions for the precisely opposite cases of $z_r = 0.2$ and $z_r = 1.2$ (the field at $z = z_t$ with $z_r = 0.2$ is equal to that at $z = 1$ with $z_r = 1.2$ and *vice versa*). Just as for the case of decreasing z_r below z_t, increasing z_r above 1 strengthens the poloidal field and again causes an increase in the horizontal scale of the most unstable modes.

4. The nonlinear regime

In this section we study the nonlinear evolution of the instability and the effects of the resulting large-amplitude motions on the magnetic layer. In particular we wish to address how the evolution is affected by changes in the strength of the poloidal field and by changes in its distribution. We consider here both linear and quadratic initial distributions of poloidal field given respectively by

$$B_x = \delta B(\xi - \xi_r), \tag{4.1a}$$

$$B_x = \delta B \frac{(\xi - \xi_r)|\xi - \xi_r|}{(1-\xi_r)^2 + \xi_r^2}, \tag{4.1b}$$

where $\xi = (z - z_t)/(1 - z_t)$ and δB measures the total excursion of B_x across the magnetic layer. Quadratic initial profiles were chosen to emphasize the effects of the resonant layer – however, as in §3.2, we found that for the parameters considered the difference between linear and parabolic distributions was small. Six representative cases, whose properties are summarized in table 1, have been chosen for discussion. In cases (i)–(iii) the total twist, as measured by δB above, is constant but the distribution of B_x varies, whereas in cases (iv)–(vi) the magnetic twist is varied for a fixed value of ξ_r. All the calculations started from a static polytropic state and the instability was triggered by a small white-noise perturbation of the temperature field.

4.1. *Variations in distribution*

We begin by discussing the effects of varying the distribution of poloidal field. It was argued in I that the nonlinear evolution of the system was controlled to a large extent by two factors; the tendency for light, magnetized fluid to rise, thereby

Case	NX	NZ	B_x	δB	ξ_r	C_k	β
i	256	128	quad.	0.4	0.05	0.05	0.2
ii	256	128	quad.	0.4	0.95	0.05	0.2
iii	256	128	linear	0.4	−0.25	0.05	0.2
iv	128	64	linear	0.4	0.50	0.07	0.5
v	128	64	linear	0.8	0.50	0.07	0.5
vi	128	64	linear	1.5	0.50	0.07	0.5

TABLE 1. Properties of numerical solutions. NX and NZ are the number of collocation points in the horizontal and vertical directions respectively. The other parameters are: $\gamma = \frac{5}{3}$, $m = 1.6$, $\theta = 2$, $\sigma = 0.05$, $\tau = 0.01$. The aspect ratio for all six cases was 2:1.

contributing positive buoyancy work, and by the formation of vortices by a secondary Kelvin–Helmholtz instability whose interactions dominated the flow in the later stages of the instability. In order to understand the evolution in the present situation we must consider how each factor might be affected by a varying poloidal field.

Clearly the impact on the buoyancy force is minimal since in a compressible fluid buoyancy is a pressure effect and therefore depends only on the modulus of $\boldsymbol{B}$ – on the other hand the effects on the secondary instability are profound. When the field is purely toroidal neighbouring fluid elements transfer momentum amongst each other by viscous stresses (neglecting the stratification) and consequently no long-range communication exists between distant regions of fluid on the dynamical timescale ($\ll$ viscous timescale). Two simple consequences of this fact are that the instability develops on the smallest horizontal scale compatible with dissipation and that the (velocity) shear at the interface between magnetized and unmagnetized fluid becomes unstable to the secondary Kelvin–Helmholtz instability. The only factor hindering the secondary instability is the stable stratification (Chandrasekhar 1961) whose effectiveness, however, can be greatly reduced if the Prandtl number is small (Zahn 1983 and references therein). A poloidal field on the other hand provides a very efficient mechanism for momentum transfer since Alfvén waves can now propagate across the layer. Distant fluid elements can thus be coupled with an effectiveness that depends on the (poloidal) field strength. A distribution of poloidal field can thus be regarded as a distribution in effective coupling between fluid particles. In this context the resonant surface is of special importance since in its neighbourhood the Alfvén crossing time (in the x,z-plane) is large and the fluid is virtually uncoupled. Furthermore, so long as the topology of the resonant surface is preserved, fluid elements on opposite sides of it cannot be coupled in the above sense. It should be noted that the coupling, being mediated by the field lines, is not between physical locations but between actual Lagrangian fluid elements and therefore evolves as the instability evolves.

Bearing these considerations in mind we inspect the numerical solutions for the first three cases of table 1. Cases (i) and (ii) have a quadratic distribution of poloidal field with, respectively, a resonant layer near the magnetic interface and near the lower boundary. In case (iii) the poloidal field increases linearly with depth and never vanishes for $z \geqslant z_t$ (no resonant layer). The time evolution for these three cases is captured by figures 6–8 (plates 1–3) which show density plots of the toroidal field intensity at four different times. Overlaying the density plots are the contours of the poloidal flux function which give the projection of the lines of force onto the (x,z)-plane. It is apparent that the three cases differ strikingly in three important respects:

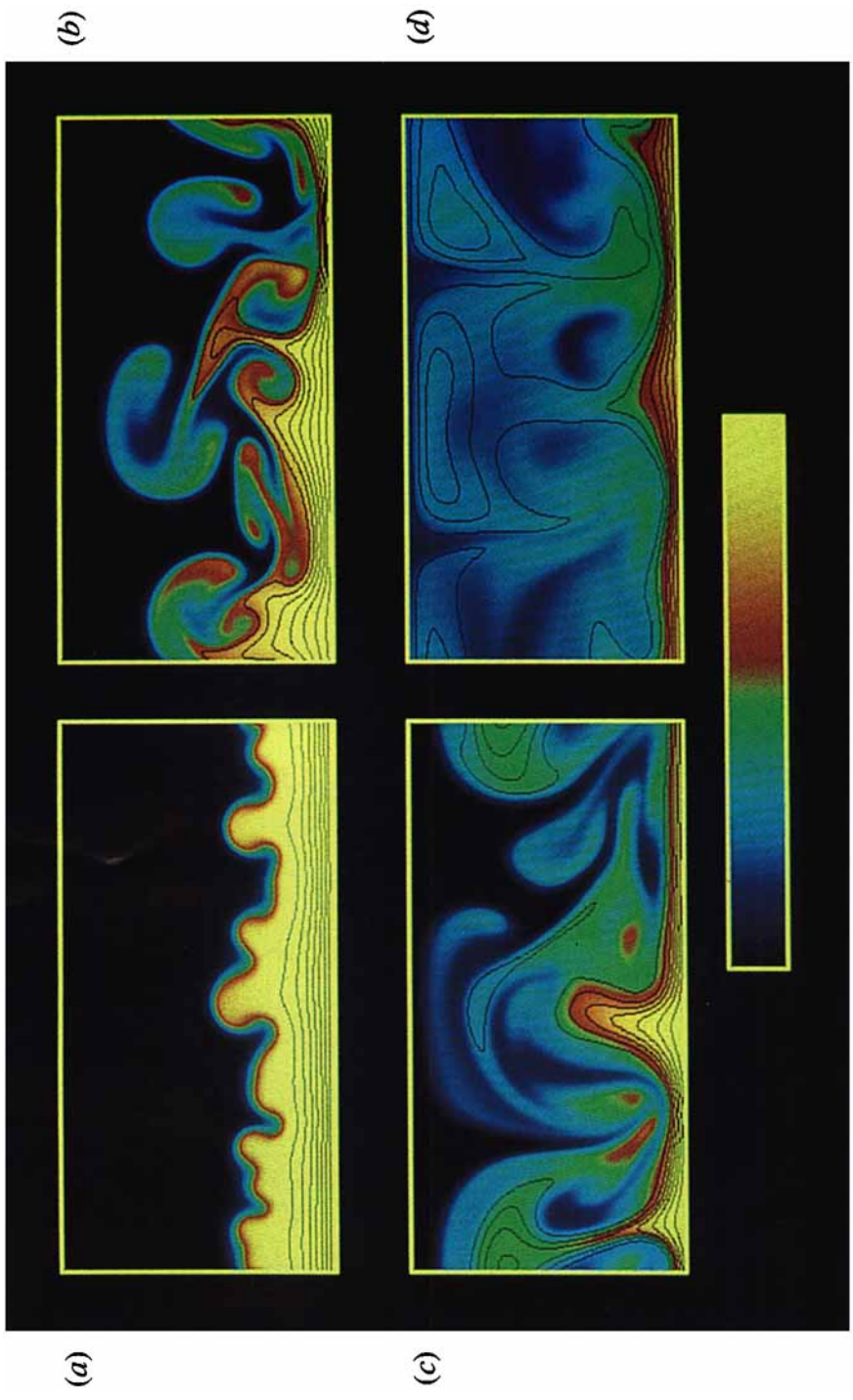

FIGURE 6. Shown in colour is the evolution of the toroidal component of the magnetic field for case (i). Regions of no toroidal field are black, regions of maximum field strength yellow. The full range of colours is shown by the colour bar. The overlying black lines are the contours of the poloidal flux function. The four frames correspond to: (*a*) $t = 2.27$, (*b*) $t = 4.16$, (*c*) $t = 5.687$ and (*d*) $t = 8.70$.

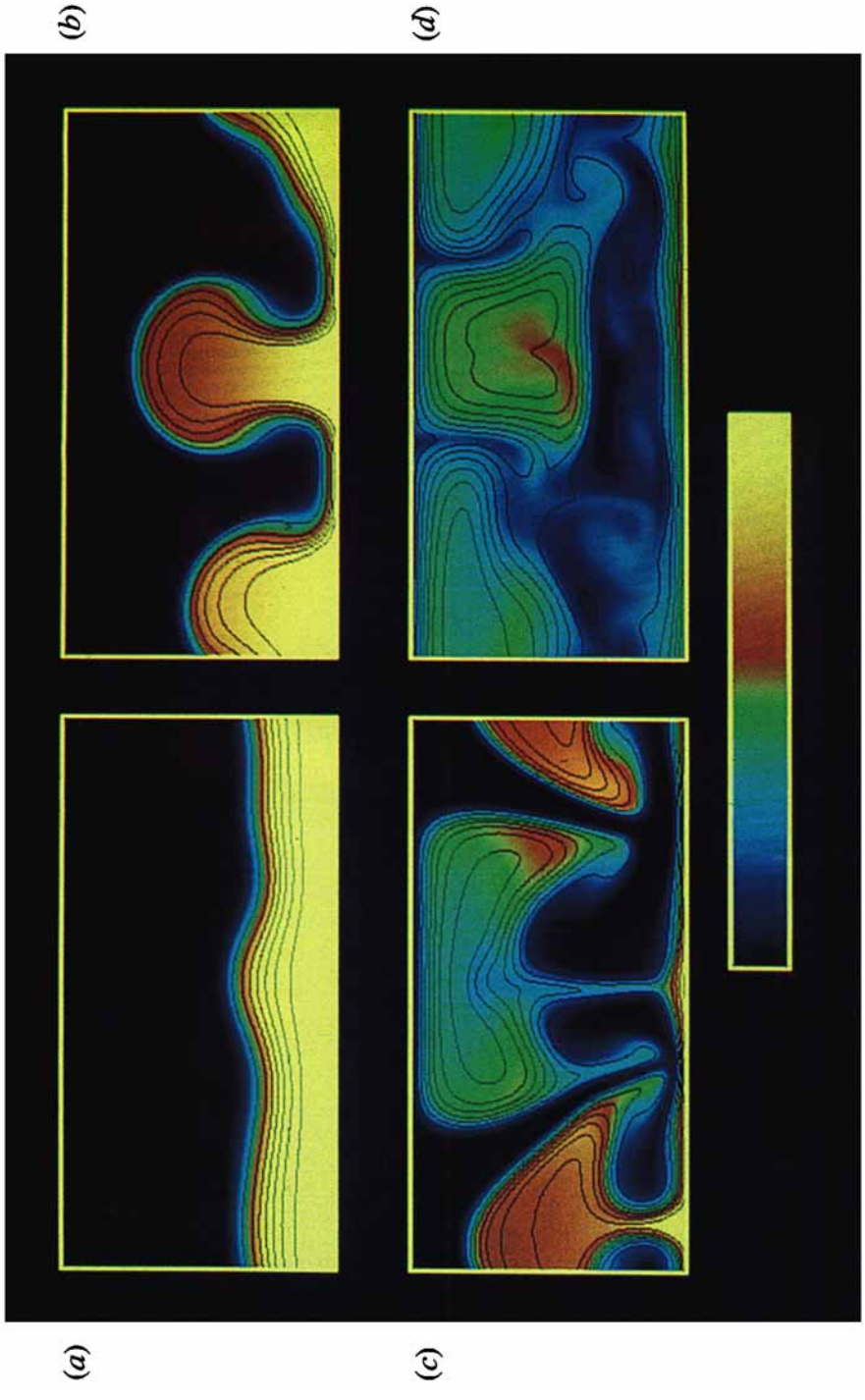

FIGURE 7. In colour is the evolution of the toroidal component of the magnetic field for case (ii). The black lines are the poloidal field lines. The four frames correspond to: (*a*) $t = 2.27$, (*b*) $t = 4.16$, (*c*) $t = 5.687$ and (*d*) $t = 8.70$.

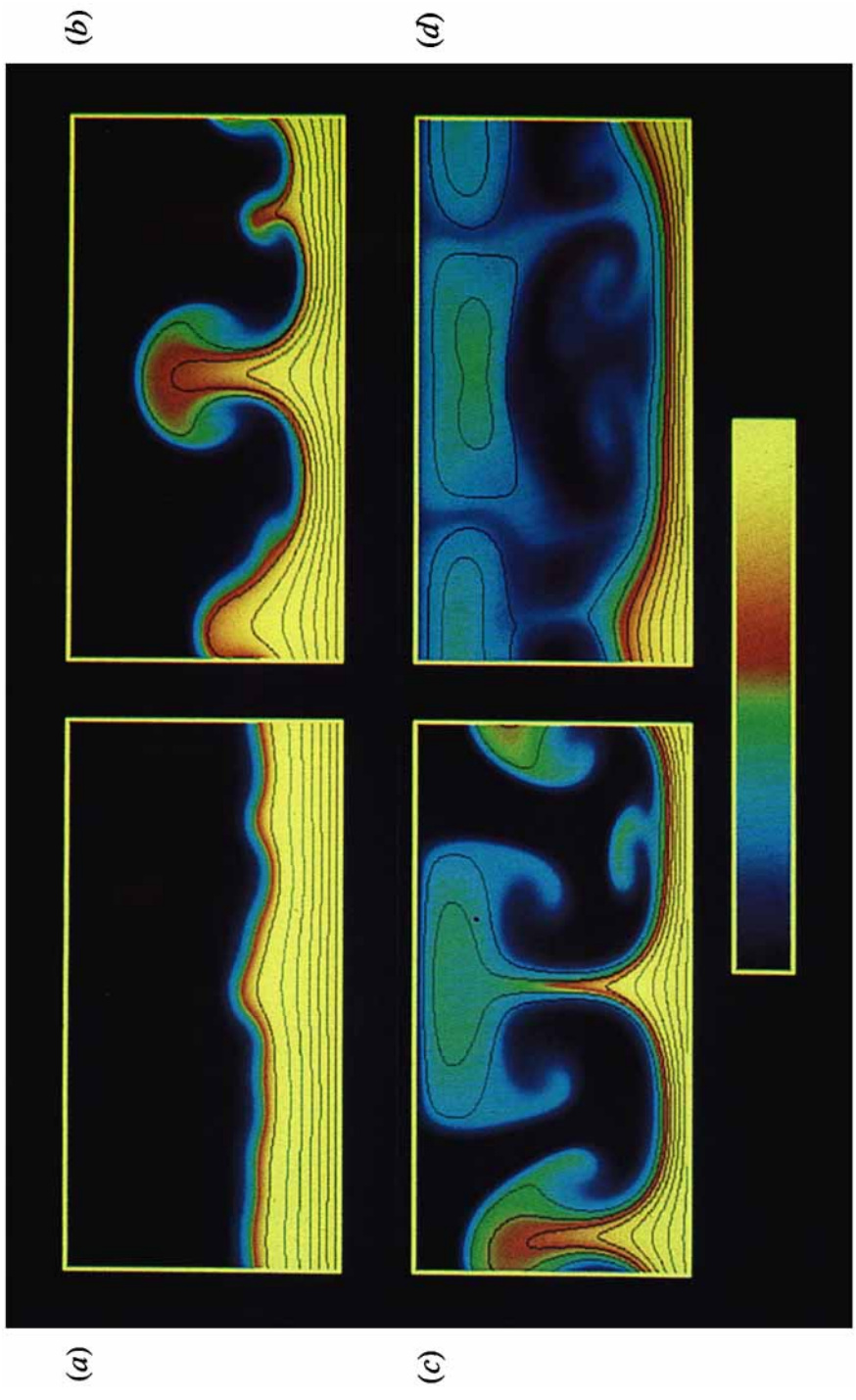

FIGURE 8. In colour is the evolution of the toroidal component of the magnetic field for case (iii). The black lines are the poloidal field lines. The four frames correspond to: (*a*) $t = 2.27$, (*b*) $t = 4.16$, (*c*) $t = 5.687$ and (*d*) $t = 8.70$.

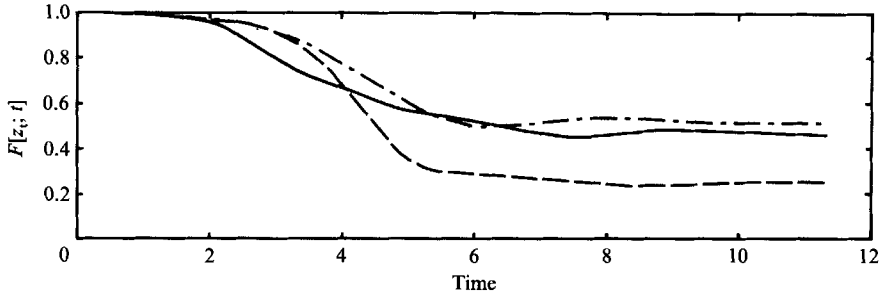

FIGURE 9. Fraction of the initial toroidal flux below z_t as a function of time. The solid line corresponds to case (i), the dashed line to case (ii) and the dot-dashed line to case (iii).

(*a*) in the spatial scales of the instability, (*b*) in the effectiveness of the instability at disrupting the magnetic layer, and (*c*) in the structure of the magnetic 'fragments' produced by the instability.

When the resonant layer is near the interface (case (i)), the instability develops on small horizontal scales and over a region of limited vertical extent. The penetration by the motions into the lower part of the layer is hindered by the increasing strength of the poloidal field and thus part of the layer escapes disruption. In figure 6(*d*) remnants of the initial layer are visible, stabilized against further disturbances by the combined action of the poloidal field and of the lower boundary (see discussion in §3.1). When the resonant layer is near the lower boundary, as it is in case (ii), the instability develops on larger scales (in case (i) between 8 and 9 bumps can be distinguished at the magnetic interface whereas only 2 are present in case (ii)) that reach down to the resonant surface and lead to the complete disruption of the layer. Very little field remains in the lower part of the domain in figure 7(*d*). In case (iii) where there is no resonant surface and B_x increases downwards the instability initially develops on relatively small scales since the poloidal field is weak near the interface but subsequently evolves to large scales as the motions grow to larger amplitude and feel the effects of the poloidal field at greater depths. In this case a substantial fraction of the initial magnetic field remains near the lower boundary.

A useful quantity to make some of these notions more quantitative is afforded by $F[z;t]$, defined to be the fraction of the initial toroidal flux below some depth z, namely

$$F[z;t] = \frac{\int_z^1 B_y(x,t)\,\mathrm{d}x}{\int_z^1 B_y(x,0)\,\mathrm{d}x}. \tag{4.2}$$

The graphs of F for $z = z_t$ shown in figure 9 give a measure of the long term resilience of the layer against the instability. By the time most of the dynamically interesting phases have occurred, case (ii) (resonance near the lower boundary) has about 20% of the initial toroidal flux in the region below z_t, whereas in cases (i) and (iii) over 50% of the initial flux still remains. The exact values of these quantities obviously depends on the choice of depth considered – for a larger value of z, 0.8 say, F is even lower for case (ii) and even higher for cases (i) and (iii). The picture that emerges from these observations is one where the resonant layer plays a dual role: on the one hand layers with a resonant surface near the magnetic interface are more easily destabilized (in the sense that a weaker field can lead to instability); on the other hand, for such

cases the motions are confined to a shallow region near the interface and the disruption of the magnetic layer is limited. By comparison, a layer with a deep resonant surface is harder to destabilize but once instability is possible it leads to the complete disruption of the magnetic region. This kind of behaviour is indeed hinted at by linear theory.

The magnetic fragments resulting from the instability also differ greatly amongst the three cases. Besides the obvious difference in size we notice a more fundamental difference in evolution. In case (i) the small corrugations formed at the interface by the instability grow into the familiar mushrooms which become unstable to the secondary Kelvin–Helmholtz instability, leading to a very effective mixing of the ejected flux. In figure 6(*d*) it is almost impossible to relate different magnetized regions in the upper part of the domain with the mushrooms at an earlier time. The homogenization of the field occurs, mainly, because the ejected field is only weakly twisted and, hence, field lines can be interchanged efficiently. In case (ii) the fragments produced by the instability retain their identity for the entire simulation. The enhanced stability of the fragments in this case is associated with the distribution of poloidal field within the fragments themselves. By inspection of figures 6 and 7 it is possible to conclude that when the initial gradient of B_x is positive (increasing downwards) the fragments produced tend to have the strongest poloidal field near their centres; contrariwise, when the gradient is negative the strongest poloidal field is found near the fragments' surfaces. Since the secondary instability is caused by the velocity shear between the rising magnetized fragment and the descending unmagnetized fluid a poloidal field concentrated at the interface is most effective at preventing the secondary instability. A measure of this effectiveness is provided by linear theory (Chandrasekhar 1961; however, see Chiueh & Zweibel 1987) which indicates that a velocity difference comparable to the parallel Alfvén speed is necessary for the secondary instability to succeed. In a way it is as if the magnetic layer and the fragments have swapped stability; a deep resonant surface causes a substantial fraction of the magnetic layer to be destroyed but the fragments produced in the process are very stable to subsequent disruption; on the other hand, for a shallow resonant surface the instability leaves some of the initial layer intact but the fragments produced are strongly affected by further instabilities.

4.2. *Variations in intensity*

We now discuss cases (iv) to (vi) which illustrate the effects of increasing the intensity of the magnetic shear. For these cases the initial distribution of poloidal field is linear and the resonant surface is in the middle of the magnetic region. The evolution is partly described in figure 10 which shows the distribution of toroidal field at two different times for each case. The black lines are part of the grey-scale plotting routine and should not be identified with the contours of the poloidal flux function. The most striking feature is again the difference in scales which, at least initially, is in good agreement with linear theory.

Figure 11 shows the time history of the average kinetic and magnetic energy densities with the contributions arising from the poloidal (meridional) and toroidal (azimuthal) components displayed separately. A number of important processes characterizing different stages of the evolution can be identified with various features of these curves. Initially potential energy is released and the amplitude of the instability grows roughly exponentially with a growth rate that is well predicted by linear theory. The differences in growth rates for the three cases are evident in figure 11(*c*) where the stronger the shear the longer the time for the instability to grow to

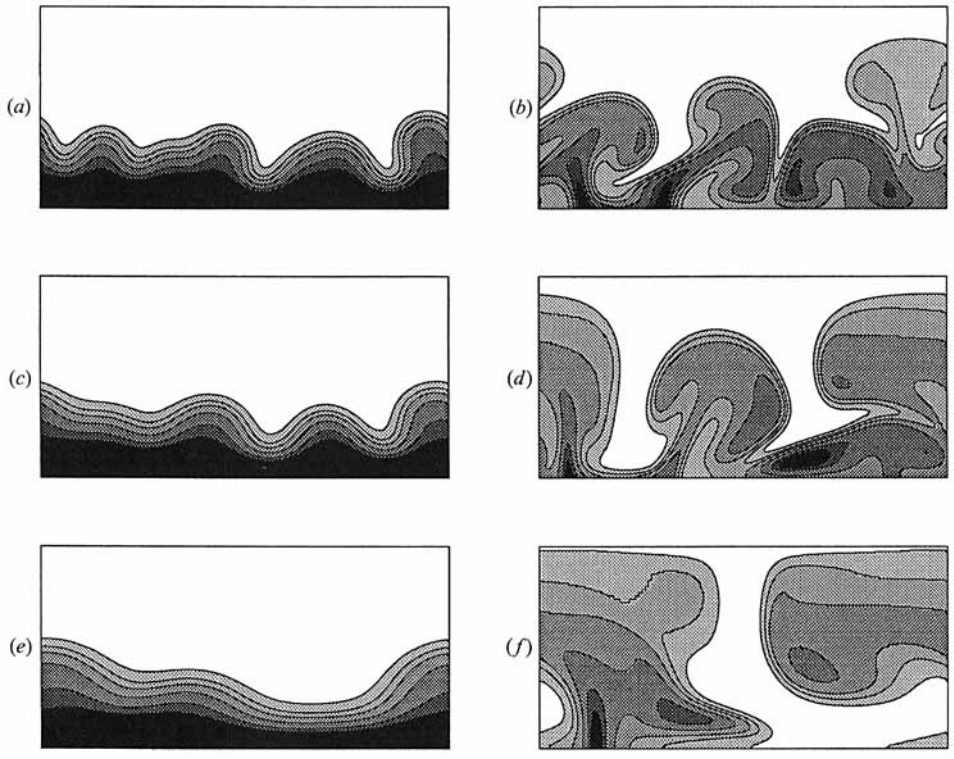

FIGURE 10. Shaded contours of the toroidal field. The figures correspond to: (*a*) case (iv), $t = 4.95$; (*b*) case (iv), $t = 8.50$; (*c*) case (v), $t = 5.84$; (*d*) case (v), $t = 10.30$; (*e*) case (vi), $t = 7.64$ and (*f*) case (vi), $t = 13.88$.

appreciable amplitude. At the same time the magnetic energy is decreasing (figure 11*b*), partly owing to the instability but mostly because of the effect of magnetic diffusion which acts to smear out the initial sharp interface between magnetized and unmagnetized fluid. This diffusive process is decoupled from the motions (initially) and is not really part of the instability but, rather, manifests the lack of a true equilibrium. As discussed in I, a magnetic layer of the type considered here satisfies the equations of thermal equilibrium and hydrostatic balance but is not a static solution of the induction equation when the magnetic diffusivity is non-zero. The change in slope in the curves describing the magnetic energy occurs when the advection of magnetic field by the fluid motions dominates over the diffusive processes and signals the beginning of the nonlinear phase of the instability. It is interesting to notice that in this second phase the contributions to the magnetic energy from the toroidal component decrease monotonically with time while the poloidal contributions exhibit peaks. These local maxima in fact reflect the amplification of poloidal field by the winding and stretching of the field lines due to meridional motions.

Zonal motions, whose contributions to the kinetic energy density are shown in figure 11(*d*), are driven exclusively by magnetic tension, which requires a non-zero poloidal component, consistent with the ordering of the curves where the amplitude of the azimuthal flow increases with increasing magnetic shear. Somewhat less obvious is a similar ordering found in figure 11(*c*), implying that the contribution to the kinetic energy due to meridional flows, and therefore the overall vigour of the

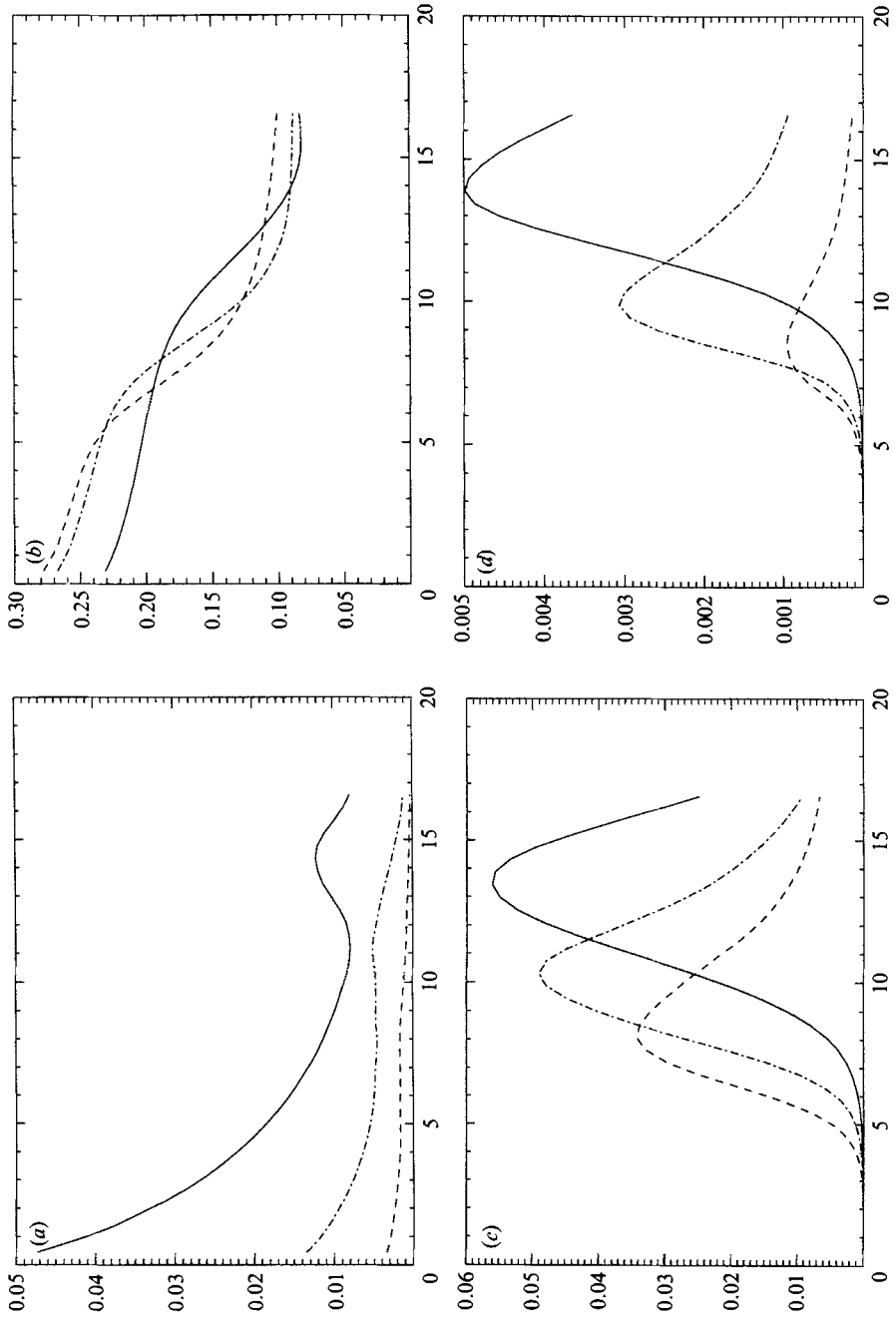

FIGURE 11. Magnetic and kinetic energy densities as functions of time. The figures correspond to: (*a*) contributions from the poloidal component of the magnetic field, (*b*) contributions from the toroidal component, (*c*) contributions from the meridional part of the flow and (*d*) contributions from the azimuthal part. Dashed lines correspond to case (iv), dot-dashed lines to case (v) and solid lines to case (vi).

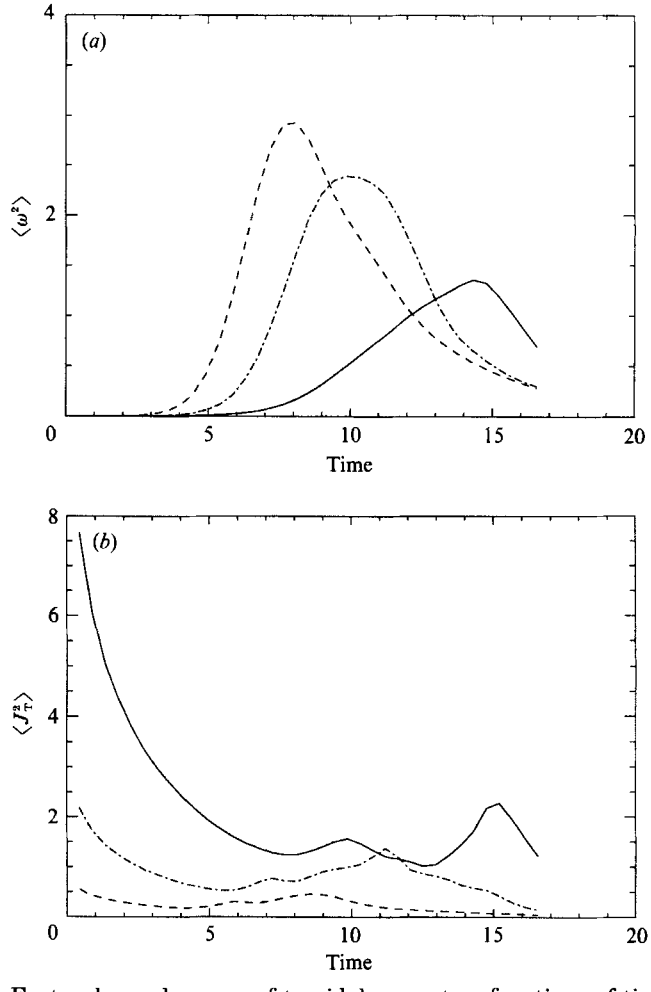

FIGURE 12. Enstrophy and square of toroidal current as functions of time. Dashed lines correspond to case (iv), dot-dashed lines to case (v) and solid lines to case (vi).

instability, also increases with increasing shear. What makes this result surprising is, once again, the dual role played by the shear; stabilizing in linear theory where growth rate decreases with increasing δB but destabilizing in the nonlinear regime where the largest amplitude motions belong to the case with the largest shear.

In order to understand this last result it is necessary to consider the mechanisms by which energy is dissipated. As we shall see presently the effective dissipation is due mainly to the formation of current sheets, which is greatly affected by the shear. Of the three dissipative mechanisms available to the system, viscous, magnetic and thermal diffusion, only the first two are important since the temperature field never develops gradients large enough for thermal damping to be significant. Their relative effectiveness can be measured by the enstrophy ($\omega^2 = |\boldsymbol{\nabla} \times \boldsymbol{u}|^2$) and by the square of the toroidal current ($J_T^2 = |\hat{\boldsymbol{y}} \cdot \boldsymbol{\nabla} \times \boldsymbol{B}|^2$). It is crucial to realize that only the toroidal component of the current is important for the dissipation of kinetic energy. This can be seen by considering an ideal decay experiment where a circulating, solenoidal flow in the (x, z)-plane advects a uniform toroidal field in an unstratified medium. In this case the flow decays due to viscosity but is almost completely insensitive to magnetic

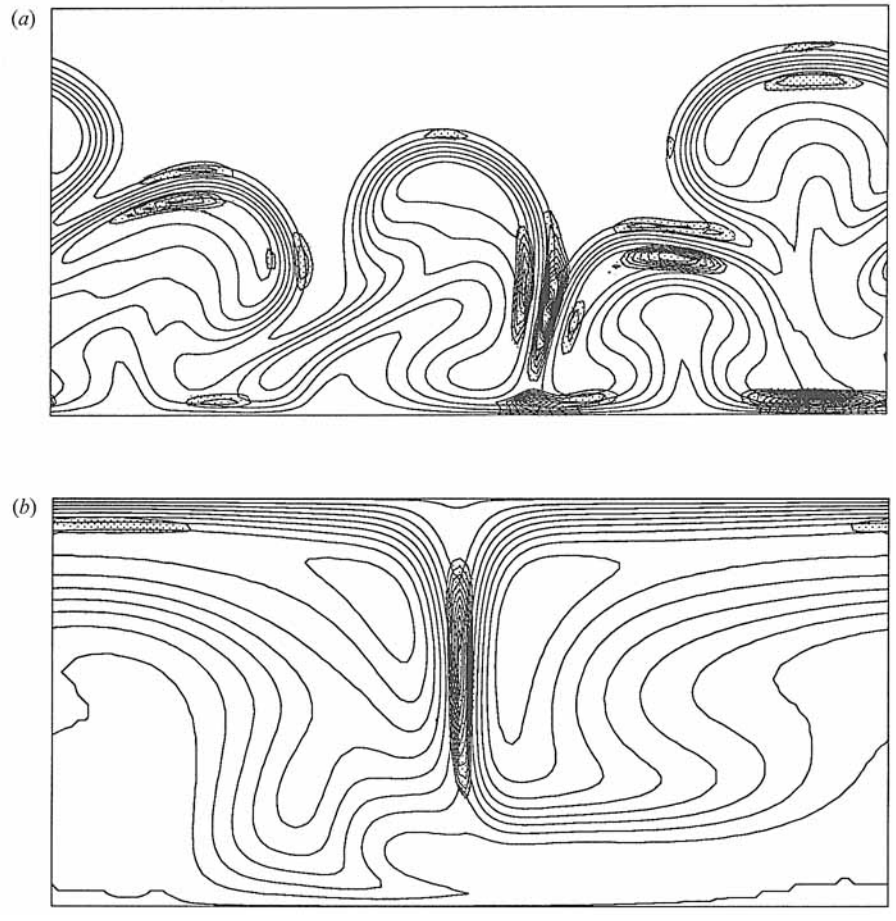

FIGURE 13. Contours of the poloidal flux function (poloidal field lines) and contours of J_T^2 (shaded regions). Only the values of J_T^2 above 10% of its maximum have been contoured. The figures correspond to: (*a*) case (v), $t = 10.4$ and (*b*) case (vi), $t = 15.21$.

diffusion except, possibly, through the coupling to magnetosonic waves which is exceedingly weak for substantially sub-Alfvénic flows. On the other hand if the field is initially poloidal the problem is one of flux expulsion, which is known to be a highly dissipative process even in the absence of viscosity (Parker 1963; Weiss 1966; Moffatt & Kamkar 1983). The main difference is that in the second case the deformation of field lines by the flow allows kinetic energy to be converted into magnetic energy which can then be dissipated Ohmically.

Figure 12 shows the time histories of $\langle \omega^2 \rangle$ and $\langle J_T^2 \rangle$ for cases (iv)–(vi). In order to obtain the relative energy dissipation rates $\langle J_T^2 \rangle$ should be multiplied by a factor of 10 which is the appropriate value of $\sigma\beta/\tau$ (see the right-hand side of (2.7)). It is clear from these curves that as the shear increases magnetic diffusion provides the dominant form of dissipation – in case (iv) Ohmic and viscous dissipation are comparable, in case (vi) their ratio is roughly 20:1.

The spatial distribution of J_T^2 however is highly intermittent with all the dissipation confined to thin current sheets. The structure of these current sheets can be seen in figure 13 where contours of J_T^2 (shaded regions) have been overlaid on contours of the poloidal flux function for cases (iv) and (vi). It is clear that the

current sheets typically form late in the evolution when the mushrooms collide either with the boundary or with each other. The first of these two events is obviously artificial and follows from the limitations of our computational domain; the second however is physically meaningful and depends on the number density of mushrooms and on the complexity of the flow, two factors that are profoundly affected by variations in shear. As the shear becomes stronger the preferred horizontal scale for the instability increases, thereby leading to a decrease in the number density of mushrooms (per unit length). Also, for weak shear the motions in the nonlinear regime are dominated by the interaction between vortices, leading to a complicated flow with a high collision rate. For stronger shear the poloidal field is very effective at hindering the secondary instability and the flow is considerably simpler with the mushrooms rising vertically and expanding. We see that as the shear becomes more important the dissipation becomes less effective at limiting the growth of the instability since current sheets are less likely to form. For example, in figure 13(*a*) a number of current sheets are present even though the magnetic interface has not yet reached the upper boundary, whereas in figure 13(*b*) the single sheet in the middle of the domain has formed owing to the lateral expansion of the mushrooms after the magnetic field has filled all available space. It is conceivable that in the absence of an upper boundary the formation of current sheets might be delayed indefinitely if the shear is sufficiently strong.

5. Conclusion

In this paper we have extended our study of instabilities driven by magnetic buoyancy to the case of a sheared magnetic layer. In contrast to paper I, where the magnetic field was treated effectively as a scalar, here we have kept the important characteristic of a vector field, albeit within the limitations of an axisymmetric treatment. The presence of a weak poloidal component introduces a new dynamical ingredient, namely tension, which leads to richer physical behaviour. Of particular relevance is the notion of the resonant surface where the tension vanishes locally.

One of the motivations of the present work concerns the storage of the solar toroidal field for times long compared to the dynamical timescale so as to allow amplification by dynamo action. It appears that when the resonant surface is located close to the interface only a small fraction of the total field is affected by the instability, leaving behind a stable layer with no resonant surface. By contrast, when the resonant surface is seated deeply within the magnetic region the nonlinear phases of the instability lead to the complete disruption of the layer. In the solar case some measure of stability could therefore be achieved by a poloidal field with a shallow resonant surface which allowed some of the flux to escape but which, on the whole, preserved the integrity of the magnetic layer.

The detailed nature of the motions is also affected by the position of the resonant surface. We observe that the development of the instability in the presence of a shallow resonant surface is similar to that for pure interchange modes with the later stages of the evolutions dominated by a secondary Kelvin–Helmholtz instability. On the other hand, when the resonant layer is deep the presence of a substantial amount of poloidal field at the interface between magnetized and field-free fluid leads to the suppression of the secondary instability and to a much more coherent evolution of the motions. The difference between these two cases is particularly apparent in the structure of the magnetic fragments produced by the instability. In the former case the magnetic field is strongly advected by the random motions generated by the

Kelvin–Helmholtz instability, leading to the efficient homogenization of the field. In this case the magnetic mushrooms generated by the initial instability are distorted by the motions and very rapidly lose their identity. In the latter case the helical structure of the magnetic mushrooms helps to prevent further disruption of the fragments. These results suggest that some of the observed modulations in scale, morphology and amplitude of the emerging flux (Golub *et al.* 1981) might be related to small variations in the distribution of the poloidal field during the solar cycle.

Another new feature deriving from the presence of tension is magnetic reconnection and the resulting coupling of kinetic energy to Ohmic dissipation. We found that, typically, magnetic reconnection occurred in one of two situations; when mushrooms detach themselves from the layer and when they collide with each other. During these events intense, localized current sheets form that lead to Ohmic dissipation. The role of Ohmic dissipation in quenching the instability depends on the overall intensity of the poloidal field, and three distinct regimes can be distinguished. When the poloidal field is very weak, tension forces are not effective enough to couple the motions to the (poloidal) field which is essentially kinematic and the dominant dissipative mechanism is viscous. This is always the case for pure interchange modes. The next regime is achieved when the poloidal field is no longer kinematic so that meridional motions couple to Ohmic dissipation but the field is not strong enough to suppress the secondary instability. Finally, in the third regime the motions and Ohmic dissipation are strongly coupled but tension forces cause a more ordered evolution with fewer events leading to the formation of current sheets.

The work in this paper has benefitted from numerous discussions with T. Bogdan, E. DeLuca, R. Rosner, T. Tajima, J. Toomre, N. Weiss and E. Zweibel. We should also like to thank the referees for their comments on the paper. This work was partially supported by the National Science Foundation through grant ATM8506632, by the National Aeronautics and Space Administration through grants NSG-7511 and NAGW-91 and by Trinity College, Cambridge. Part of this work was carried out during visits by D. W. Hughes to Boulder and F. Cattaneo to Cambridge. We are grateful to Professor J. Toomre for arranging the former and to Professor N. O. Weiss for arranging, and to the SERC for supporting the latter.

REFERENCES

Bernstein, I. B., Frieman, E. A., Kruskal, M. D. & Kulsrud, R. M. 1958 An energy principle for hydromagnetic stability problems. *Proc. R. Soc. Lond.* A **244**, 17–40.

Cattaneo, F. & Hughes, D. W. 1988 The nonlinear breakup of a magnetic layer: instability to interchange modes. *J. Fluid Mech.* **196**, 323–344 (referred to as I herein).

Chandrasekhar, S. 1961 *Hydrodynamic and Hydromagnetic Stability*. Clarendon.

Chiueh, T. & Zweibel, E. G. 1987 The structure and dissipation of forced current sheets in the solar atmosphere. *Astrophys. J.* **317**, 900–917.

Golub, L., Rosner, R., Vaiana, G. S. & Weiss, N. O. 1981 Solar magnetic fields: the generation of emerging flux. *Astrophys. J.* **243**, 309–316.

Hughes, D. W. & Cattaneo, F. 1987 A new look at the instability of a stratified horizontal magnetic field. *Geophys. Astrophys. Fluid Dyn.* **39**, 65–81.

Kulsrud, R. M. 1964 General stability theory in plasma physics. In *Advanced Plasma Theory, Proc. of the Intl School of Physics XXV* (ed. M. N. Rosenbluth), pp. 54–96. Academic.

Moffatt, H. K. & Kamkar, H. 1983 The time-scale associated with flux expulsion. In *Planetary and Stellar Magnetism* (ed. A. M. Soward), pp. 91–97. Gordon and Breach.

Parker, E. N. 1963 Kinematical hydromagnetic theory and its application to the low solar photosphere. *Astrophys. J.* **138**, 552–575.

ROSENBLUTH, M. N., DAGAZIAN, R. Y. & RUTHERFORD, P. H. 1973 Nonlinear properties of the internal $m = 1$ kink instability in the cylindrical tokamak. *Phys. Fluids* **16**, 1894–1902.

SUYDAM, B. R. 1958 Stability of a linear pinch. In *Proc. 2nd UN Intl Conf. on Peaceful Uses of Atomic Energy*, vol. 31, pp. 157–159.

WEISS, N. O. 1966 The expulsion of magnetic flux by eddies. *Proc. R. Soc. Lond.* A **293**, 310–328.

WHITE, R. 1983 Resistive instabilities and field lines reconnection. In *Handbook of Plasma Physics, Vol. I* (ed. A. A. Galeev & R. N. Sudan), pp. 611–676. North-Holland.

ZAHN, J.-P. 1983 Instability and mixing processes in upper main sequence stars. In *Astrophysical Processes in Upper Main Sequence Stars* (ed. A. N. Cox, S. Vauclair & J.-P. Zahn), pp. 253–329. Geneva Observatory.